Bose-Einstein correlations and v_{2n} and v_{2n-1} in hadron and nucleus collisions

E. Gotsman,[1,*] E. Levin,[1,2,†] and U. Maor[1,‡]

[1]*Department of Particle Physics, School of Physics and Astronomy, Raymond and Beverly Sackler Faculty of Exact Science, Tel Aviv University, Tel Aviv, 69978, Israel*

[2]*Departemento de Física, Universidad Técnica Federico Santa María, and Centro Científico- Tecnológico de Valparaíso, Avda. Espana 1680, Casilla 110-V, Valparaíso, Chile*

(Received 31 July 2016; revised manuscript received 21 December 2016; published 8 February 2017)

We show that Bose-Einstein correlations of identical particles in hadron and nucleus high-energy collisions, lead to long-range rapidity correlations in the azimuthal angle. These correlations are inherent features of the CGC/saturation approach, however, their origin is more general than this approach. In framework of the proposed technique both even and odd v_n occur naturally, independent of the type of target and projectile. We are of the opinion that it is premature to conclude that the appearance of azimuthal correlations are due to the hydrodynamical behavior of the quark-gluon plasma.

DOI: 10.1103/PhysRevD.95.034005

One of the most intriguing experimental observations made at the LHC and RHIC, is the occurrence of the same pattern of azimuthal angle correlations in the three types of interactions: hadron-hadron, hadron-nucleus and nucleus-nucleus collisions. In all three reactions, correlations in the events with large density of produced particles, are observed between two charged hadrons, which are separated by large values of rapidity [1–7], these correlations do not depend on the rapidity separation of the particles. Due to causality arguments [8], two hadrons with large difference in rapidity between them, could only correlate at the early stage of the collision and, therefore, we expect that the correlations between two particles with large rapidity difference (at least the correlations in rapidity) are due to the partonic state with large parton density. The CGC/saturation approach (see [9] for a review) appears to be a natural candidate for the description of these correlations, as these correlations are significant in the dense colliding systems. However, unlike the large rapidity correlations, the azimuthal angle correlations can originate from the collective flow in the final state [10]. At first sight, this source appears even more plausible, since v_n with odd n do not appear in the CGC/saturation approach.

In this article, we show that the long-range rapidity correlations in the azimuthal angle, arise naturally from the Bose-Einstein correlations of produced identical particles in high-energy collisions. They originate from the initial state wave function of the colliding particles, and they are features characteristic of the CGC/saturation approach. However, their occurrence is more general, and can be estimated in other frameworks. In this paper, we estimate these correlations in the framework of the Pomeron calculus. We will show that this approach leads to the azimuthal correlations, with the correlation length (R_c), which increases with energy (s) being proportional to $R_c^2 \propto \alpha'_{\mathbb{P}} \ln s/s_0$.[1] Due to such a large correlation length, these correlations do not depend on the transverse momenta behavior of different vertices of Pomeron interactions, which have only phenomenological sources in the Pomeron calculus. We will estimate the values of v_n, and demonstrate that v_n with odd n appear naturally in this framework.

In the framework of the Pomeron calculus, the long-range rapidity correlations stem from the production of two parton showers (see Fig. 1). The structure of the parton shower is described by the exchange of a Pomeron, while the upper and lower blobs in Fig. 1(c) as well as the vertex of parton emission require modeling in the framework of the Pomeron calculus. However, if two produced patrons have the same quantum numbers, we need to take into account interference diagrams [see Fig. 2(a) and Fig. 2(b)], which lead to an additional Mueller diagram [12] of Fig. 2(c) in which two partons with $(y_1, \boldsymbol{p}_{T2})$ and $(y_1, \boldsymbol{p}_{T1})$ are produced. When $\boldsymbol{p}_{T1} \to \boldsymbol{p}_{T2}$, the two production processes become identical, leading to the cross section $\sigma(\text{two identical patrons}) = 2\sigma(\text{two different partons})$, as one expects. However, when $|\boldsymbol{p}_{T2} - \boldsymbol{p}_{T1}| \gg 1/R$ where R is the size of the emitter, the interference diagram becomes small and can be neglected.

For the general case of $y_1 \neq y_2$, the interference diagram has a more complicated structure than the Mueller diagram of Fig. 2(c). The general parton diagrams are shown in Fig. 3(a) and Fig. 3(b) for the case of $\Delta|y_2 - y_2| \gg 1$. In the parton approach, the emission of every parton leads to the factor Δy_i, where Δ is the Pomeron intercept, and y_i is the rapidity difference of the order of $\Delta Y \gg 1$. In the diagram of Fig. 3(a) and Fig. 3(b), we can see that the emitted partons for each parton shower can be divided in three groups:

*gotsman@post.tau.ac.il
†leving@post.tau.ac.il, eugeny.levin@usm.cl
‡maor@post.tau.ac.il

[1]The soft Pomeron trajectory has the form: $\alpha(t) = 1 + \Delta + \alpha'_{\mathbb{P}}|t|$ with the intercept $\Delta = 0.1$–0.14 and the slope $\alpha'_{\mathbb{P}} = 0.2$–$0.32$ GeV^{-2} from high-energy phenomenology [11].

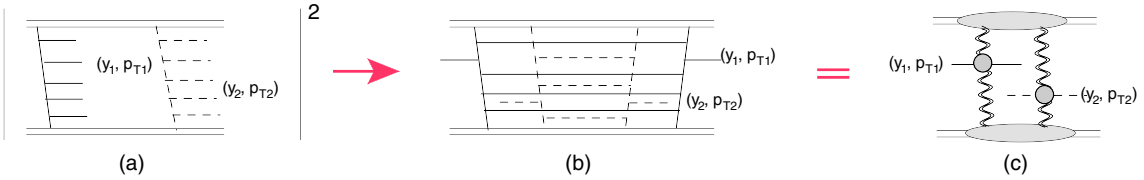

FIG. 1. Production of two patrons with $(y_1, \boldsymbol{p}_{T1})$ and $(y_2, \boldsymbol{p}_{T2})$ in two parton showers, (a) and (b); (c) shows the Mueller diagrams [12] for the double inclusive cross section. The wavy lines denote the soft Pomerons.

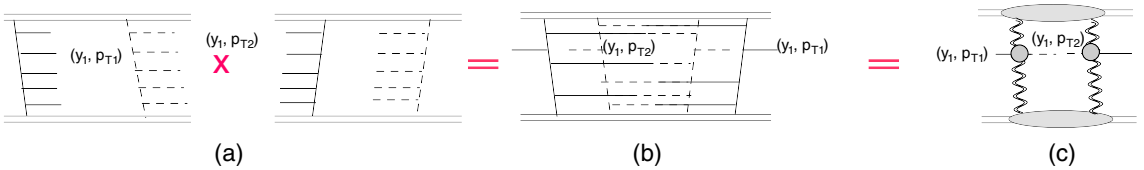

FIG. 2. Production of two identical partons with $(y_1, \boldsymbol{p}_{T1})$ and $(y_1, \boldsymbol{p}_{T2})$ in two parton showers (a) and (b). The diagrams in the Mueller diagram technique [12] are shown in (c). The wavy lines denote the soft Pomerons [13,14].

$$\text{first parton shower} \to Y > \underbrace{\ldots > y_i > \ldots > y_{n^{(1)}}}_{n_1^{(1)}} > y_1 > \underbrace{y_{n^{(1)}+1} > \ldots}_{n_2^{(1)}} > y_2 > \underbrace{> y_i > \ldots}_{n_3^{(1)}} > 0;$$

$$\text{second parton shower} \to Y > \underbrace{\ldots > y_i > \ldots > y_{n^{(2)}}}_{n_1^{(2)}} > y_1 > \underbrace{y_{n^{(2)}+1} > \ldots}_{n_2^{(2)}} > y_2 > \underbrace{> y_i > \ldots}_{n_3^{(2)}} > 0. \tag{1}$$

Integrating over y_i, and neglecting y_i dependence of the production amplitude [13,14], we obtain the contribution

$$\frac{d\sigma}{dy_1 d^2p_{T1} dy_2 d^2p_{T2}} = \sum_{n_1^{(1)}+n_2^{(1)}+n_3^{(1)}-2>2}^{\infty} \sum_{n_1^{(2)}+n_2^{(2)}+n_3^{(2)}-2>2}^{\infty} \int d\Phi^{(1)} d\Phi^{(2)} |A(\{y_i, p_{Ti}\}; y_1, p_{T1}; y_2, p_{T2})|^2$$

$$= \sum\sum \underbrace{\frac{(\Delta(Y-y_1))^{n_1^{(1)}}}{n_1^{(1)}!} \frac{(\Delta(Y-y_1))^{n_1^{(2)}}}{n_1^{(2)}!} \frac{(\Delta(y_1-y_2))^{n_2^{(1)}}}{n_2^{(1)}!} \frac{(\Delta(y_1-y_2))^{n_2^{(2)}}}{n_2^{(2)}!} \frac{(\Delta(y_2-0))^{n_3^{(1)}}}{n_3^{(1)}!} \frac{(\Delta(y_2-0))^{n_3^{(2)}}}{n_3^{(2)}!}}_{\text{integral over longitudinal phase space}}$$

$$\times \int \prod_i d^2p_{Ti} |A(\{y_i = 0, p_{Ti}\}; y_1 = 0, p_{T1}; y_2 = 0, p_{T2})|^2 \tag{2}$$

where $d\Phi^{(1)}$ and $d\Phi^{(2)}$ denote the phase space of the produced partons in the first and second parton showers.

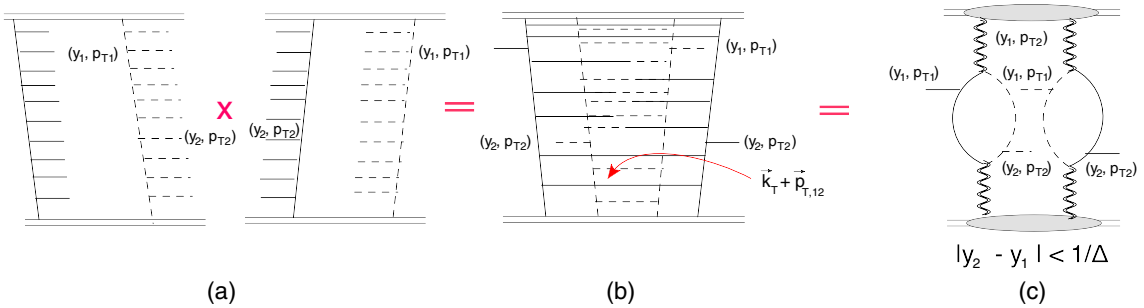

FIG. 3. Production of two identical partons with $(y_1, \boldsymbol{p}_{T1})$ and $(y_2, \boldsymbol{p}_{T2})$ for $\Delta|y_2 - y_1| \gg 1$ in two parton showers (a) and (b); (a) shows the Mueller diagram [12] for $\Delta)|y_2 - y_1| \ll 1$. The Pomeron intercept $\alpha_{\mathbb{P}} = 1 + \Delta$. The wavy lines denote the soft Pomerons [13,14].

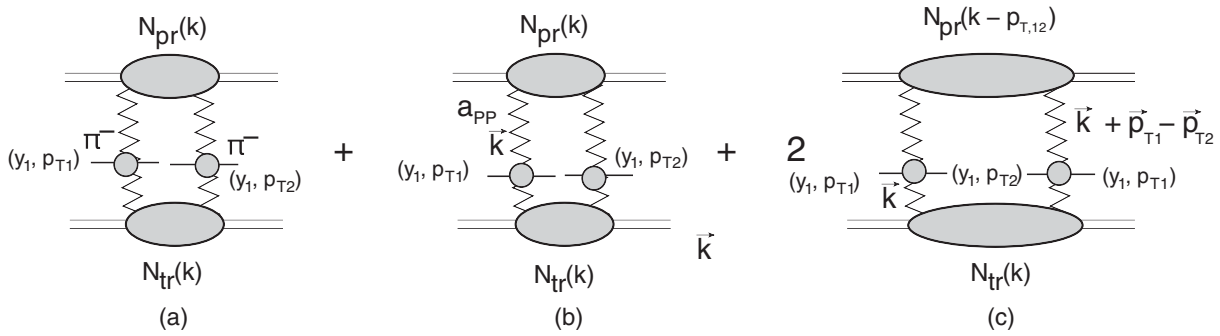

FIG. 4. The Mueller diagrams for production of two identical π^- with $(y_1, \boldsymbol{p}_{T1})$ and $(y_1, \boldsymbol{p}_{T2})$, in two parton showers [see (a)–(c)]. The zigzag lines denote the soft Pomerons.

The cross section of Eq. (2) displays several general features:

(1) Equation (2) shows the factorization of the longitudinal and transverse degrees of freedom, which is the principle characteristic of the parton approach, as well as LLA of QCD [13,14].

(2) After summation over $n_i^{(1)}$ and $n_i^{(2)}$, the cross section turns out to be proportional to $\exp(\Delta(2(Y-y_1)+2(y_1-y_2)+2(y_2-0))) = \exp(2\Delta Y)$, and it does not depend on y_1 and y_2.

(3) The factorization allows us to rewrite the general formula for the correlation of the identical particles [15] with the coordinates $\boldsymbol{r}_1$ and $\boldsymbol{r}_2$:

$$\frac{d^2\sigma}{dy_1 dy_2 d^2p_{T1} d^2p_{T2}}(\text{identical partons}) \propto \langle 1 + e^{i r_\mu Q_\mu}\rangle, \tag{3}$$

where averaging $\langle\ldots\rangle$ includes the integration over $r_\mu = r_{1,\mu} - r_{2,\mu}$. For $y_1 = y_2$ $Q_\mu = p_{1,\mu} - p_{2,\mu}$ degenerates to $\boldsymbol{Q} \equiv \boldsymbol{p}_{T,12}$. Due to factorization of the longitudinal and transverse degrees of freedom in Eq. (2), the amplitude can be written in the factorized form $A = A_L(r_+, r_-)A_T(\boldsymbol{r}_T)$ leading to

$$\langle e^{i r_\mu Q_\mu}\rangle = \underbrace{\langle e^{i \boldsymbol{r}_T \cdot \boldsymbol{Q}_T}\rangle}_{\text{averaging over } r_T} \times \underbrace{\langle e^{i r^+ Q_- + i r^- Q_+}\rangle}_{\text{averaging over } r_+, r_-}. \tag{4}$$

The first factor is a constant with respect to y_1 and y_2, since the cross section does not depend on the rapidities of the emitted partons.

(4) From Eq. (2), we can conclude that the emission of partons with rapidities $y_2 < y_i < y_1$ give negligible contributions for $\Delta(y_1 - y_2) \ll 1$. Since the phenomenological value [11] for $\Delta = 0.1$–0.14, we can simplify our approach for wide range of rapidities $|y_1 - y_2| < 1/\Delta \approx 7$–$10$. For such rapidities, Fig. 3(b) can be reduced to the Mueller diagram of Fig. 3(c), which has the same expression as the Mueller diagram of Fig. 2(c), since the transverse amplitudes $A(\{y_i = 0, p_{Ti}\}; y_1 = 0, p_{T1}; y_2 = 0, p_{T2})$ in Eq. (2) are the same in these two cases.

Therefore, to recover the correlation function, we can restrict ourselves to calculating the cross section at $y_1 = y_2$. The cross section for double pion production has the following generic form (see Fig. 4):

$$\begin{aligned}\frac{d^2\sigma}{dy_1 dy_2 d^2p_{T1} d^2p_{T2}}&(\text{identical pions}) \\ &= \frac{d^2\sigma}{dy_1 dy_2 d^2p_{T1} d^2p_{T2}}\,[\text{Fig.4(a) and (b)}] \\ &\quad + \frac{d^2\sigma}{dy_1 dy_2 d^2p_{T1} d^2p_{T2}}\,[\text{Fig.4(c)}] \qquad (5)\end{aligned}$$

$$\begin{aligned}&= \frac{d^2\sigma}{dy_1 dy_2 d^2p_{T1} d^2p_{T2}}(\text{different pions}) \\ &\quad \times [1 + C(R|\boldsymbol{p}_{T2} - \boldsymbol{p}_{T1}|)] \qquad (6)\end{aligned}$$

The second term in Eq. (5) describes the interference diagram in which one π^- is produced in one parton shower, but it is absorbed by another parton shower. $C(R|\boldsymbol{p}_{T2} - \boldsymbol{p}_{T1}|)$ is the correlation function we wish to calculate.

The angular correlation of two idential pions stems from the diagram of Fig. 4(c) (see diagrams of Fig. 2(c) and Fig. 3(c) for partons) where the upper BFKL Pomerons carry momentum $\boldsymbol{k}_T - \boldsymbol{p}_{T,12}$ with $\boldsymbol{p}_{T,12} = \boldsymbol{p}_{T1} - \boldsymbol{p}_{T2}$, while the lower BFKL Pomerons have momenta $\boldsymbol{k}_T$. As has been mentioned in this article, we demonstrate a mechanism for the appearance of these angular correlations in the framework of a simple approach: the soft Pomeron calculus.[2] The Mueller diagrams for the correlation between two π^- are shown in Fig. 4. This approach is based on Gribov Pomeron

[2]The correlation of identical particles was investigated in the framework of the soft Pomeron calculus and the mechanism of the azimuthal angle correlation that we discuss here, has been proposed in Ref. [16] for hadron and nucleus interactions. Recently, it has been re-discovered in Ref. [17] in the framework of the CGC approach. We revisit this formalism for calculations of v_n for odd and even n.

calculus [18] and the Mueller diagram technique [12], which has a general origin in the analyticity and unitarity of strong interaction (see [19]) and which has been proven in the leading log approximation of perturbative QCD [20]. The exchange of the soft Pomeron leads to the following contribution to the elastic scattering amplitude [19]

$$A_{\rm el}(Y,k_T) = i g_{\rm pr}(k_T) g_{\rm tr}(k_T) P(Y,k_t)$$

with the Pomeron propagator

$$P(Y,k_t) = e^{\Delta_{\mathbb{P}} - \alpha'_{\mathbb{P}} Y k_T^2}, \tag{7}$$

where $\Delta_{\mathbb{P}}$ and $\alpha'_{\mathbb{P}}$ denote the intercept and slope of the Pomeron trajectory, and from the phenomenological description of experimental data have the values $\Delta_{\mathbb{P}} = 0.1$–$0.14$ and $\alpha'_{\mathbb{P}} = 0.1$–$0.25\ \text{GeV}^{-2}$ (see Ref. [11]). Vertices $g_{\rm pr}(k_T)$ and $g_{\rm tr}(k_T)$ can only be functions of k_T. Their dependence on k_T^2 cannot be found in the framework of the Reggeon approach, but the exponential form is used in the phenomenology that describes the current experimental data on soft interaction [11], viz.,

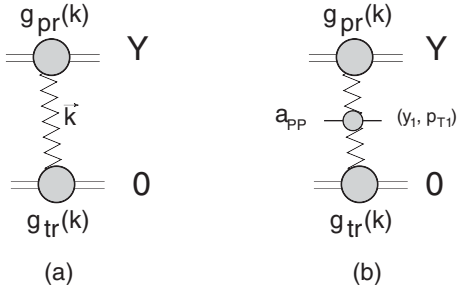

FIG. 5. The contribution of the Pomeron exchange to the elastic scattering amplitude at momentum transferred k^2 (a) and the Mueller diagram for the inclusive production of a pion at rapidity y_1 and transverse momentum p_{T1} (b).

$$g_{\rm pr}(k_T) = g^0_{\rm pr} e^{-\frac{1}{2} B^0_{\rm pr} k_T^2}; \qquad g_{\rm tr}(k_T) = g^0_{\rm tr} e^{-\frac{1}{2} B^0_{\rm tr} k_T^2}. \tag{8}$$

As we will show below, the azimuthal angle correlations do not depend on the form of the parametrization of the Pomeron vertices. The inclusive cross section is described by the Mueller diagram of Fig. 5(b), and it takes the form

$$\begin{aligned}\frac{d\sigma}{dy_1 d^2 p_{T1}} &= g_{\rm pr}(k_T=0) g_{\rm tr}(k_t=0) a_{\mathbb{P}\mathbb{P}}(p_{T1}) P(Y-y_1, k_T=0) P(y_1, k_T=0)\\ &= g_{\rm pr}(k_T=0) g_{\rm tr}(k_t=0) a_{\mathbb{P}\mathbb{P}}(p_{T1}) P(Y, k_T=0)\end{aligned} \tag{9}$$

One can see that the inclusive cross section does not depend on rapidity y_1, which corresponds to the production of pions in a one parton shower.

The sum of the diagrams of Fig. 4 can be written as

$$\begin{aligned}&\left.\frac{d\sigma}{dy_1 d^2 p_{T1} dy_2 d^2 p_{T2}}\right|_{y_1=y_2}\\ &= 2\int d^2k_T N_{\rm pr}(k_T) P(Y-y_1,k_T) a_{\mathbb{P},\mathbb{P}}(p_{T1},k_T) P(y_1,k_T) P(Y-y_1,k_T) a_{\mathbb{P},\mathbb{P}}(p_{T2},k_T) P(y_1,k_T) N_{\rm pr}(k_T)\\ &\quad + 2\int d^2k_T N_{\rm pr}(\boldsymbol{k}_T - \boldsymbol{p}_{T,12}) P(Y-y_1, \boldsymbol{k}_T - \boldsymbol{p}_{T,12}) a_{\mathbb{P},\mathbb{P}}(p_{T1},p_{T2},k_T) P(y_1,k_T)\\ &\quad \times P(Y-y_1, \boldsymbol{k}_T - \boldsymbol{p}_{T,12}) a_{\mathbb{P},\mathbb{P}}(p_{T1},p_{T2},k_T) P(y_1,k_T) N_{\rm pr}(k_T)\\ &= 2e^{2\Delta_{\mathbb{P}} Y}\int d^2k_T \{N_{\rm pr}(k_T) a_{\mathbb{P},\mathbb{P}}(p_{T1},k_T) a_{\mathbb{P},\mathbb{P}}(p_{T2},k_T) N_{\rm tr}(k_T) e^{-2\alpha'_{\mathbb{P}} Y k_T^2}\\ &\quad + N_{\rm pr}(\boldsymbol{k}_T - \boldsymbol{p}_{T,12}) a^2_{\mathbb{P},\mathbb{P}}(p_{T1},p_{T2},k_T) N_{\rm tr}(k_T) e^{-\alpha'_{\mathbb{P}}(2y_1 k_T^2 + 2(Y-y_1)(\boldsymbol{k}_T - \boldsymbol{p}_{T,12})^2)}\}.\end{aligned} \tag{10}$$

The first observation that at large Y the typical k_T^2 and $|\boldsymbol{k}_T - \boldsymbol{p}_{T,12}|$ in both integrals turns out to be of the order of $1/(\alpha'_{\mathbb{P}} 2(Y-y_1)) \ll$ any dimensional parameters in $a_{\mathbb{P}\mathbb{P}}$ and N. In other words, both k_T and $p_{T,12}$ are proportional to $1/(\alpha'_{\mathbb{P}} Y)$ which make them smaller than the typical values of the radii, both in the Pomeron-hadron vertices and in vertex $a_{\mathbb{P}\mathbb{P}}$. Therefore, we can neglect the k_T and $p_{T,12}$ dependences of the vertices. From the second term, one can see that $p^2_{T,12} \sim 1/(2\alpha'_{\mathbb{P}}(Y-y_1)) \ll p^2_{2T}$ and p^2_{1T}. Hence, at ultrahigh energies, the double inclusive cross section for identical pions is equal:

$$\left.\frac{d\sigma}{dy_1 d^2 p_{T1} dy_2 d^2 p_{T2}}\right|_{y_1=y_2} = 2N^2(0) a^2_{\mathbb{P}\mathbb{P}}(p_{T1}) e^{2\Delta_{\mathbb{P}} Y} \frac{1}{2\alpha'_{\mathbb{P}} Y}\left\{1 + \exp\left(-2\alpha'_{\mathbb{P}} \frac{(Y-y_1)y_1}{Y} p^2_{T,12}\right)\right\} \tag{11}$$

Therefore, at ultrahigh energy, the azimuthal angle (ϕ) dependence is determined by (i) the correlation length $R_c^2 = 2\alpha'_{\mathbb{P}} \frac{(Y-y_1)y_1}{Y}$ and since $p_{T,12}^2 \sim 1/R_c^2 \ll \mu^2$, where μ is the sale of soft interaction which does not depend on energy, the correlations do not depend on the form of the vertices and $N(Q_T)$, which can only be treated phenomenologically in the framework of the Pomeron calculus, (ii) no symmetry with respect to $\phi \to -\phi$, and (iii) Eq. (11) includes all the powers of $\cos\phi$ and, therefore, we obtain v_n with both even and odd n.

For realistic estimates, we need to use a more phenomenological approach. The amplitude $N(Q_T)$ can be written in the form [11] (see Fig. 6):

$$N_{\rm tr}(Q_T) = \underbrace{g^2_{\rm tr}(Q_T)}_{\text{eikonal contribution}} + \underbrace{g^2_{{\rm tr},D}(Q_T)}_{\text{diffraction contribution}} . \quad (12)$$

For the simplest estimates, we take into account only the first term in Eq. (12). In other words, we use the eikonal model for estimates of the amplitude for two soft Pomeron production. In the case of the nucleus target and/or projectile, this corresponds to the Glauber model.

For the vertices of the soft Pomeron interaction with the projectile and target we use Eq. (8), and for the vertex of pion emission from the Pomeron we use the simplest parametrization:

$$a_{\mathbb{PP}}(p_{T1}, p_{T2}) = a^0_{\mathbb{PP}} e^{-\frac{1}{2}B_e(p^2_{T1}+p^2_{T2})}. \quad (13)$$

We have neglected the possible dependence of $a_{\mathbb{PP}}$ on k^2, as follows from the phenomenological models [11], and on $\boldsymbol{p}_{T,12}$. It should be stressed that the more general form, for example $a_{\mathbb{PP}}(p_{T1}, p_{T2}) = a^-_{\mathbb{PP}}(\boldsymbol{p}_{T1} - \boldsymbol{p}_{T2}) a^+_{\mathbb{PP}} \times (\boldsymbol{p}_{T1} + \boldsymbol{p}_{T2})$, even in the case when $a^-_{\mathbb{PP}} = a^+_{\mathbb{PP}}$ and this vertex is symmetric with respect to $\phi \to -\phi$, as has been suggested in perturbative QCD [17], does not change the conclusion that the resulting expression has no such symmetry.

In the eikonal approximation, the contribution of the interference diagram of Fig. 4(c) to the double inclusive cross section for $y_1 = y_2$ is equal to

$$\frac{d\sigma}{dy_1 d^2p_{T1} dy_2 d^2p_{T2}} = a^2_{\mathbb{PP}}(p_{T1}, p_{T2}) e^{2\Delta_{\mathbb{P}}Y} \frac{(g^0_{\rm pr})^2 (g^0_{\rm tr})^2}{4\pi^2} \int d^2k_T \exp(-B_{\rm tr}k_T^2 - B_{\rm pr}(\boldsymbol{k}_T - \boldsymbol{p}_{T,12})^2)$$
$$= (a^0_{\mathbb{PP}})^2 \frac{(g^0_{\rm pr})^2 (g^0_{\rm tr})^2}{4\pi(B_{\rm tr} + B_{\rm pr})} e^{2\Delta_{\mathbb{P}}Y} \exp(-(B_e + B_R)(p^2_{T1} + p^2_{T2}) - 2B_R p_{T1} p_{T2} \cos(\varphi)), \quad (14)$$

where

$$B_R = \frac{B_{\rm pr} B_{\rm tr}}{B_{\rm pr} + B_{\rm tr}}. \quad (15)$$

Recall that $B_{\rm pr} = B^0_{\rm pr} + \alpha'_{\mathbb{P}}(Y - y_1)$ and $B_{\rm tr} = B^0_{\rm tr} + \alpha'_{\mathbb{P}} y_1$.

The sum of all diagrams of Fig. 4 leads to

$$\frac{d\sigma}{dy_1 d^2p_{T1} dy_2 d^2p_{T2}} = (a^0_{\mathbb{PP}})^2 \frac{(g^0_{\rm pr})^2 (g^0_{\rm tr})^2}{4\pi(B_{\rm tr} + B_{\rm pr})} e^{2\Delta_{\mathbb{P}}Y} \exp(-B_e(p^2_{T1} + p^2_{T2}))\{1 + \exp(-B_R(p^2_{T1} - 2p_{T1}p_{T2}\cos(\varphi) + p^2_{T2}))\}. \quad (16)$$

The expansion of Eq. (16) contains all powers of $\cos(\varphi)$ or, in other words, all $\cos(n\varphi)$ with even and odd n.

We can rewrite Eq. (16) in terms of the observables which can be measured: the slopes of elastic scattering and the rapidity correlation function $C(y_1, y_2)$ defined as

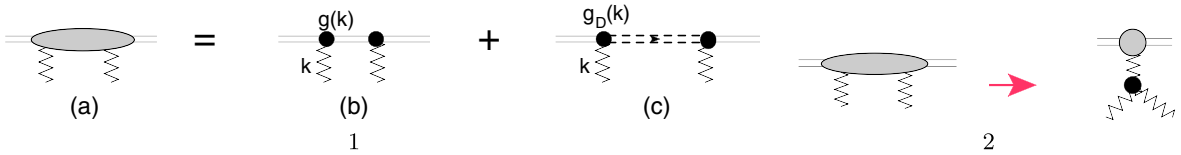

FIG. 6. The structure of the Pomeron-proton amplitude: (1b) figure illustrates the contribution of the eikonal approach, while (1c) gives the diffraction dissociation contribution, and (2) shows the contribution to $N(k_T)$, the production of large mass. The black blob in (2) denotes the triple Pomeron vertex.

$$C(y_1,y_2)=\frac{1}{\sigma_{\rm in}}\int d^2p_{T1}d^2p_{T2}\frac{d\sigma}{dy_1d^2p_{T1}dy_2d^2p_{T2}}\Big/\left(\frac{1}{\sigma_{\rm in}}\int d^2p_{T1}\frac{d\sigma}{dy_1d^2p_{T1}}\right)\left(\frac{1}{\sigma_{\rm in}}\int d^2p_{T2}\frac{d\sigma}{dy_2d^2p_{T,2}}\right). \quad (17)$$

It is more convenient to introduce a correlation function $C(y_1,p_{T1};y_2,p_{T2})$ as

$$\begin{aligned}C(y_1,p_{T1};y_2,p_{T2})&=\frac{\frac{1}{\sigma_{\rm in}}\frac{d\sigma}{dy_1d^2p_{T1}dy_2d^2p_{T2}}}{(\frac{1}{\sigma_{\rm in}}\frac{d\sigma}{dy_1d^2p_{T1}})(\frac{1}{\sigma_{\rm in}}\frac{d\sigma}{dy_2d^2p_{T2}})}\\&=C(y_1,y_2)\left\{1+\frac{B_R}{B_R+B_e}\exp(-B_R(p_{T1}^2-2p_{T1}p_{T2}\cos(\varphi)+p_{T2}^2))\right\}. \quad (18)\end{aligned}$$

Using

$$\int_0^{2\pi}d\varphi e^{2p_{T1}p_{T2}\cos(\varphi)}\cos(n\varphi)=2\pi I_n(2p_{T1}p_{T2}), \quad (19)$$

where $I_n(z)$ is the modified Bessel function of the first kind, we will decompose the term in $\{\ldots\}$ in $C(y_1,p_{T1};y_2,p_{T2})$ into Fourier modes in the relative azimuthal angle φ between two produced pions:

$$\begin{aligned}&C(y_1,p_{T1};y_2,p_{T2})\propto 1+2\sum_{n=1}V_{n\Delta}(p_{T1},p_{T2})\cos(n\varphi)\\&\text{with}\quad V_{n\Delta}(p_{T1},p_{T2})=\frac{1}{2}I_n(2B_Rp_{T1}p_{T2})\frac{e^{-B_R(p_{T1}^2+p_{T2}^2)}}{1+I_0(2B_Rp_{T1}p_{T2})e^{-B_R(p_{T1}^2+p_{T2}^2)}}, \quad (20)\end{aligned}$$

assuming that $B_e\ll B_R$.

The coefficients $v_n(p_T)$ are equal to

$$v_n(p_T)=\frac{V_{n\Delta}(p_T,p_T^{\rm Ref})}{\sqrt{V_{n\Delta}(p_T^{\rm Ref},p_T^{\rm Ref})}}=\frac{1}{\sqrt{2}}\frac{I_n(2B_Rp_{T1}p_{T2}^{\rm Ref})}{\sqrt{I_n(2B_R(p_{T2}^{\rm Ref})^2)}}\frac{\sqrt{1+I_0(2B_R(p_{T2}^{\rm Ref})^2)e^{-2B_R(p_{T2}^{\rm Ref})^2}}}{1+I_0(2B_Rp_{T1}p_{T2}^{\rm Ref})e^{-B_R(p_{T1}^2+(p_{T2}^{\rm Ref})^2)}}, \quad (21)$$

where the value of $p_T^{\rm Ref}$ is determined by the experimental procedure. Fixing $p_T^{\rm Ref}=p_T$, we obtain

$$v_n(p_T)=\frac{1}{\sqrt{2}}e^{-B_Rp_T^2}\sqrt{\frac{I_n(2B_Rp_T^2)}{1+I_0(2B_Rp_T^2)e^{-2B_Rp_T^2}}}. \quad (22)$$

Equation (22) stems from the diagrams of Fig. 4. However, like-sign pion pairs contribute a third of the total contribution to pion-pair production. This means that the double inclusive cross section is equal to

$$\begin{aligned}\frac{d\sigma}{dy_1d^2p_{T1}dy_2d^2p_{T2}}&=\frac{d\sigma}{dy_1d^2p_{T1}dy_2d^2p_{T2}}\ (\text{unlike pairs})+\frac{d\sigma}{dy_1d^2p_{T1}dy_2d^2p_{T2}}\ (\text{identical pairs})\\&=\frac{d\sigma}{dy_1d^2p_{T1}dy_2d^2p_{T2}}\ (\text{unlike pairs})\left(1+\frac{1}{3}C(p_{T1};p_{T2})\right). \quad (23)\end{aligned}$$

Therefore, Eq. (22) has to be multiplied by a factor of $1/3$.

In Eq. (15) $B_{\rm pr}$ and $B_{\rm tr}$ can be expressed in terms of the slope for the elastic cross section for $y_1=y_2=Y/2$ for projectile-projectile and target-target scattering, respectively: $B_{\rm pr}=\frac{1}{2}B^{\rm el}_{\rm pr-pr}$ and $B_{\rm tr}=\frac{1}{2}B^{\rm el}_{\rm tr-tr}$.

For proton-proton scattering at W$=7$ GeV, $B_{\rm pr}=B_{\rm tr}=\frac{1}{2}B^{\rm el}_{p-p}=10\ \text{GeV}^{-2}$ [21], which leads to $B_R=5\ \text{GeV}^{-2}$. Note that the value of B_R turns out to be rather large $B_R>\mu^2$, where μ is the scale for $N(Q_T)$ and Pomeron vertices, which is less than or equal to 1 GeV^2. This fact guarantees that the form of the vertices is not essential in the estimates of v_n. However, we would like to again stress that the appearance of v_n with odd n does not depend on the structure of the vertices, but stems from the Pomeron propagator. Plugging this value into Eq. (22), we obtain the v_n shown in Fig. 7. One can see that we obtain sufficiently large values of v_n, which are concentrated at rather large values of p_T. The width of the p_T distribution will increase if we use a more complicated structure of the Pomeron-hadron amplitude (see Fig. 6) and include diffraction dissociation processes [see Fig. 6(c)], parametrizing $g_B(k)=g_D^0\exp(-\frac{1}{2}B_Dk^2)$; Eq. (22) will have the following form:

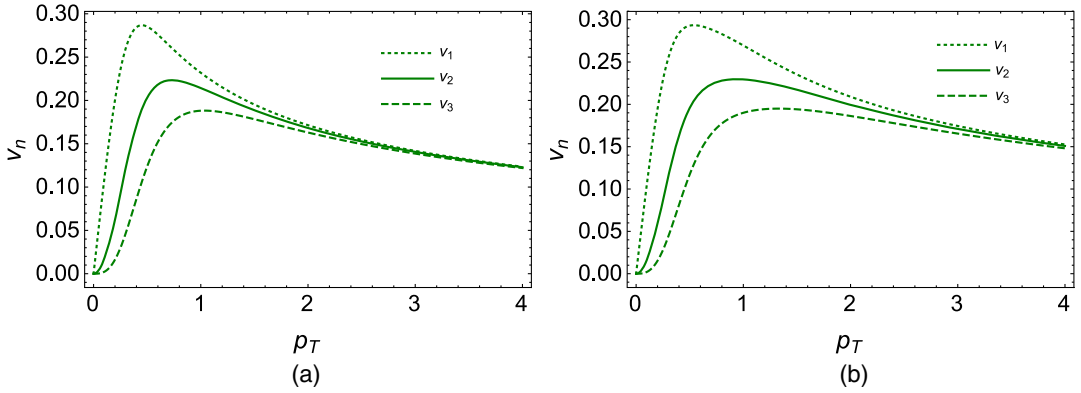

FIG. 7. v_n vs p_T using Eq. (22): (a) using the eikonal structure of Pomeron-hadron amplitude [see Fig. 6(b)] while (b) includes the process of diffraction dissociation [see Fig. 6(c)].

$$v_n(p_T) = \frac{1}{3\sqrt{2}} \sqrt{\frac{I_n(2B_R p_T^2) e^{-2B_R p_T^2} + \frac{\sigma_{sd} B_D^{sd}}{\sigma_{el} B^{el}} I_n(2B_D p_T^2) e^{-2B_D p_T^2}}{1 + I_0(2B_R p_T^2) e^{-2B_R p_T^2} + \frac{\sigma_{sd} B_D^{sd}}{\sigma_{el} B^{el}} I_0(2B_D p_T^2) e^{-2B_D p_T^2}}}, \tag{24}$$

where σ_{sd} denotes the cross section of the single diffractive production,[3] B_D^{sd} the slope of the differential cross section for diffraction dissociation is roughly equal to $\frac{1}{2}B^{el}$, B_D is the slope of Pomeron-hadron vertex for diffraction dissociation [see Fig. 6(c)]. The value of B_D has been evaluated in Ref. [23], and it is equal ≈ 1 GeV^{-2}. Figure 7(b) shows the calculation using Eq. (24) with $\frac{\sigma_{sd} B_D^{sd}}{\sigma_{el} B^{el}}$. One can see that the p_T distribution becomes broader. We need to include the diffraction contribution to $N(k_T)$ for large mass, which is related to the enhanced diagrams of Fig. 6(2). It is known that the triple Pomeron vertex has very mild dependence on the value of transverse momenta, which will be translated in a much broader distribution of v_n with respect to the transverse momentum. However, to take these diagrams into account, one needs to rely more on a model, and we postpone this to a separate paper.

In this article, our goal was not to describe the experimental data, but to demonstrate that a simple model leads to reasonable values of v_n for proton-proton scattering. From the general expression of Eq. (22), we see that the estimates are independent of the type of projectile and target. We have not attempted to obtain an estimate for hadron-nucleus and nucleus-nucleus scattering, since the Gaussian approximation for $g(k^2)$ is not suitable for these reactions. Nevertheless, in this oversimplified model, Eq. (15) shows that for the hadron-nucleus interaction, the value and p_T dependence of v_n are determined by the size of proton, rather than the size of the nucleus. Realistic estimates from a model based on CGC/saturation approach, in which we successfully described the diffractive physics, as well as main features of the multiparticle production reaction [22,24–26] will follow in the near future. We wish to point out that in the CGC approach, pions originate from the gluon jet decay, and we expect the same strength of correlations both for like-like and unlike-like pion pairs, as is seen in experiments. To illustrate this, it is sufficient to note, that the production of two like-like pairs of ρ-resonances, that dominate the inclusive production, say $\rho^0\rho^0 + \rho^+\rho^+$, generate the same numbers of $\pi^+\pi^+$ and $\pi^+\pi^-$ pairs. It is worthwhile mentioning, that we obtain the correlation function in the limited region of rapidities $y_{12} = |y_1 - y_2| < 1/\Delta$ but, since for large y_{12} the cross section of Eq. (2) does not depend on y_{12}, we believe that our estimates are valid in the wider range of rapidities.

We proposed a mechanism for the long-range rapidity azimuthal angle correlations which is general, simple, and has a clear relation to diffractive physics, unlike the hydrodynamic approach, which is suited to describe only processes of multiparticle generation. We demonstrated that this mechanism leads to a value of v_n both for even and odd n, which are of the order of measured values for proton-proton collisions. We believe that it is premature to conclude that the occurrence of angular correlations is a strong argument in support of the hydrodynamical behavior of the quark-gluon plasma.

We thank our colleagues at Tel Aviv University and UTFSM for encouraging discussions. Our special thanks go to Carlos Cantreras, Alex Kovner, and Michel Lublinsky for elucidating discussions on the subject of this paper. This research was supported by the BSF Grant No. 2012124, by Proyecto Basal FB 0821(Chile), Fondecyt (Chile) Grant No. 1140842 and by CONICYT Grant No. PIA ACT140.

[3]For our estimates, we took all cross sections from Ref. [22].

[1] V. Khachatryan *et al.* (CMS Collaboration), J. High Energy Phys. 09 (2010) 091.

[2] J. Adams *et al.* (STAR Collaboration), Phys. Rev. Lett. **95**, 152301 (2005).

[3] B. Alver *et al.* (PHOBOS Collaboration), Phys. Rev. Lett. **104**, 062301 (2010).

[4] H. Agakishiev *et al.* (STAR Collaboration), arXiv: 1010.0690.

[5] S. Chatrchyan *et al.* (CMS Collaboration), Phys. Lett. B **718**, 795 (2013).

[6] S. Chatrchyan *et al.* (CMS Collaboration), Eur. Phys. J. C **72**, 2012 (2012).

[7] M. G. Poghosyan, J. Phys. G **38**, 124044 (2011); K. Aamodt *et al.* (ALICE Collaboration), Eur. Phys. J. C **65**, 111 (2010); A. R. Timmins (ALICE Collaboration), J. Phys. G **38**, 124093 (2011); arXiv:1106.6057; J. Phys. G **38**, 124093 (2011).

[8] A. Dumitru, F. Gelis, L. McLerran, and R. Venugopalan, Nucl. Phys. **A810**, 91 (2008).

[9] Y. V. Kovchegov and E. Levin, *Quantum Choromodynamics at High Energies*, Cambridge Monographs on Particle Physics, Nuclear Physics and Cosmology (Cambridge University Press, Cambridge, England, 2012).

[10] E. V. Shuryak, Phys. Rev. C **76**, 047901 (2007); S. A. Voloshin, Phys. Lett. B **632**, 490 (2006); S. Gavin, L. McLerran, and G. Moschelli, Phys. Rev. C **79**, 051902 (2009).

[11] E. Gotsman, E. Levin, and U. Maor, Int. J. Mod. Phys. A **30**, 1542005 (2015); Y. M. Shabelski and A. G. Shuvaev, J. High Energy Phys. 11 (2014) 023; Eur. Phys. J. C **75**, 438 (2011); E. Gotsman, E. Levin, U. Maor, and J. S. Miller, Eur. Phys. J. C **57**, 689 (2008); V. A. Khoze, A. D. Martin, and M. G. Ryskin, Int. J. Mod. Phys. A **30**, 1542004 (2015); Eur. Phys. J. C **71**, 1617 (2011); M. G. Ryskin, A. D. Martin, V. A. Khoze, and A. G. Shuvaev, J. Phys. G **36**, 093001 (2009); S. Ostapchenko, Phys. Rev. D **89**, 074009 (2014); **81**, 114028 (2010).

[12] A. H. Mueller, Phys. Rev. D **2**, 2963 (1970).

[13] E. A. Kuraev, L. N. Lipatov, and F. S. Fadin, Sov. Phys. JETP **45**, 199 (1977); Y. Y. Balitsky and L. N. Lipatov, Sov. J. Nucl. Phys. **28**, 622 (1978).

[14] L. N. Lipatov, Phys. Rep. **286**, 131 (1997); Sov. Phys. JETP **63**, 904 (1986) and references therein.

[15] R. H. Brown and R. Q. Twiss, Nature (London) **178**, 1046 (1956); G. Goldhaber, W. B. Fowler, S. Goldhaber, and T. F. Hoang, Phys. Rev. Lett. **3**, 181 (1959); G. I. Kopylov and M. I. Podgoretsky, Yad. Fiz. **15**, 392 (1972) [Sov. J. Nucl. Phys. **15**, 219 (1972)]; G. Alexander, Rep. Prog. Phys. **66**, 481 (2003).

[16] E. M. Levin, M. G. Ryskin, and S. I. Troian, Yad. Fiz. **23**, 423 (1976) [Sov. J. Nucl. Phys. **23**, 222 (1976)]; A. Capella, A. Krzywicki, and E. M. Levin, Phys. Rev. D **44** (1991) 704.

[17] Y. V. Kovchegov and D. E. Wertepny, Nucl. Phys. **A906**, 50 (2013); T. Altinoluk, N. Armesto, G. Beuf, A. Kovner, and M. Lublinsky, Phys. Lett. B **752**, 113 (2016); **751**, 448 (2015).

[18] V. N. Gribov, Zh. Eksp. Teor. Fiz. **53**, 654 (1967) [Sov. Phys. JETP **26**, 414 (1968)].

[19] P. D. B. Collins, *An Introduction to Regge Theory and High Energy Physics* (Cambridge University Press, Cambridge, England, 1977).

[20] L. V. Gribov, E. M. Levin, and M. G. Ryskin, Phys. Rep. **100**, 1 (1983).

[21] F. Ferro (TOTEM Collaboration), AIP Conf. Proc. **1350**, 172 (2011); G. Antchev *et al.* (TOTEM Collaboration), Europhys. Lett. **96**, 21002 (2011); **95**, 41001 (2011); Phys. Rev. Lett. **111**, 262001 (2013).

[22] E. Gotsman, E. Levin, and U. Maor, Eur. Phys. J. C **75**, 179 (2015).

[23] H. Kowalski and D. Teaney, Phys. Rev. D **68**, 114005 (2003).

[24] E. Gotsman, E. Levin, and U. Maor, Eur. Phys. J. C **75**, 18 (2015).

[25] E. Gotsman, E. Levin, and U. Maor, Phys. Lett. B **746**, 154 (2015).

[26] E. Gotsman, E. Levin, and U. Maor, Eur. Phys. J. C **75**, 518 (2015).